Circulation: Arrhythmia and Electrophysiology

ORIGINAL ARTICLE

HCN4 Mutation Causing Familial Inappropriate Sinus Tachycardia Leads to a Conformational Change Mimicking cAMP Binding and Induces Constitutive Channel Activity

Sara L. Bober, PhD; Qiuju Li, MD; David Ros-Pardo, MSc; Trent Faultless, MSc; Íñigo Marcos-Alcalde, PhD; Paulino Gómez-Puertas, PhD; Michael H. Gollob, MD

BACKGROUND: Inappropriate sinus tachycardia (IST) is an arrhythmia characterized by rapid sinus rates of over 100 bpm at rest. The mechanisms underlying this often-debilitating condition are not fully understood. The differential diagnosis for this persistent observation is broad, including medication side effects or serendipitous use of chronotropic stimulating drugs. Genetic causes of IST are seldom considered. Only 2 mutations have been linked to this condition, both of which affect the gene encoding *HCN4* channels, which play an important role in generating pacemaker activity of the sinoatrial node.

METHODS: Standard clinical genetic testing was performed on a child with IST, her affected mother, and 2 healthy siblings. A novel *HCN4* channel variant identified in the family was studied by whole-cell patch clamp analysis. Three-dimensional protein structures of mutant and wild-type *HCN4* channels were generated and subjected to 200 ns of unrestricted molecular dynamics simulation.

RESULTS: A heterozygous, missense variant was identified in the *HCN4* gene (p.N299S) in the affected child and mother, while absent in 2 healthy siblings of the child. Patch clamp analysis revealed significantly increased *HCN4* current density and a rightward-shifted activation curve in cells expressing p.N299S-*HCN4* versus wild-type channels, suggesting constitutive activity of the mutant *HCN4* channel. In molecular dynamics simulations, the voltage sensor of p.N299S-*HCN4* channels adopted a resting conformation mimicking that of cAMP-bound wild-type *HCN4*, providing a structural basis for the functional observations. Ivabradine application returned the gain-of-function properties of mutant channels to baseline levels.

CONCLUSIONS: We identified a gain-of-function *HCN4* variant in a family with IST that displays constitutive activity and structurally mimics the effects of cAMP activation. This study furthers our understanding of the mechanisms underlying IST and provides data supporting the efficacious effect of ivabradine in genetically based IST.

GRAPHIC ABSTRACT: A graphic abstract is available for this article.

Key Words: gain-of-function mutation ■ genetics ■ hyperpolarization-activated cyclic nucleotide-gated channels ■ ivabradine ■ molecular dynamics simulation ■ sinus ■ tachycardia

Inappropriate sinus tachycardia (IST) is an arrhythmia characterized by rapid sinus rates of over 100 bpm at rest, disproportionate to physiological need. Clinical presentation of IST is highly variable, and its mechanisms and pathophysiology are not fully understood. Patients may be asymptomatic or experience a range of distressing symptoms, including palpitations, chest pain, dizziness, and anxiety.[1] Recognizing the cause of IST can be challenging and requires consideration of numerous possible etiologies, including endocrine disorders, medication side

Correspondence to: Michael H. Gollob, MD, Division of Cardiology, Department of Medicine, Department of Physiology, University of Toronto, 200 Elizabeth St., Toronto, Ontario, Canada M5G 2C4. Email michael.gollob@uhn.ca
For Sources of Funding and Disclosures, see page 915.

Circulation: Arrhythmia and Electrophysiology is available at www.ahajournals.org/journal/circep

WHAT IS KNOWN?

- Inappropriate sinus tachycardia (IST) is an arrhythmia characterized by very rapid sinus rates while at rest. Serendipitous causes are often suspected with rare consideration of a genetic component.
- HCN4 channels are essential for generating pacemaker activity of the sinoatrial node.

WHAT THE STUDY ADDS

- We report here familial IST caused by a gain-of-function mutation in the HCN4 gene with conformational tertiary structure changes mimicking cAMP binding and causing constitutive channel activity.
- This study emphasizes the importance of recognizing genetic causes of IST in clinical practice and provides data supporting the efficacious effect of ivabradine in hereditary forms of this condition.

Nonstandard Abbreviations and Acronyms

CNBD	cyclic nucleotide binding domain
HCND	HCN domain
I_{HCN4}	hyperpolarization-activated cyclic nucleotide-gated potassium channel current
IST	inappropriate sinus tachycardia
MD	molecular dynamics
WT	wild-type

effects, or serendipitous use of chronotropic stimulating drugs, often in the setting of desired weight loss.

While genetic causes are well-established for many arrhythmia syndromes, a single gene basis[2] for IST has only recently been recognized. Only 2 mutations have been linked to this condition,[3,4] both of which affect the gene encoding the *HCN4*, the molecular correlate of I_{HCN}, which is essential for generating pacemaker activity of the SA node.[5] Also known as funny channels due to their unique biophysical properties, *HCN4* channels are activated by membrane hyperpolarization and further potentiated by the second messenger cAMP, which shifts the voltage dependence of channel activation toward more depolarized potentials and accelerates channel activation while slowing deactivation.[6,7]

Herein, we describe the third mutation associated with IST, a constitutively active *HCN4* variant (p.N299S) found in a child with prenatal-onset IST and her affected mother, while absent in 2 healthy siblings of the child. Functional analysis and 3D modeling provide insight into the mechanism of mutant channel activity, unique in nature from the 2 previously described *HCN4* variants. We further provide evidence for the efficacious effect of ivabradine in suppressing channel activity in vitro and its clinical benefit in the affected patients.

METHODS

The data that support the findings of this study are available from the corresponding author upon reasonable request.

Clinical Evaluation

We studied a family in which IST had been diagnosed in a daughter and mother (Figure 1D). Genetic testing was performed in a certified laboratory for a panel of genes associated with cardiac ion channelopathies. Written informed consent was obtained from study participants under an institutionally approved research ethics protocol on inherited arrhythmia and cardiomyopathy syndromes.

cDNA Constructs

A human *HCN4* clone donated by Dane Chetkovich (*HCN4*/EGFP-C1; Addgene plasmid # 197389; http://n2t.net/addgene:197389; RRID: Addgene_197389) was subcloned into pIRES2-ZsGreen1 (Takara Bio USA, San Jose, CA) by restriction enzyme double digestion, then ligation. The c.896A>G mutation (corresponding to p.N229S) was introduced into WT *HCN4* cDNA using a modified SPRINP method[8] with Q5 Hot Start High-Fidelity 2x Master Mix (NEB M0494) and verified by Sanger sequencing.

Cell Culture and Transfection

Chinese hamster ovary cells were cultured in F12 medium with 10% FBS, 2 mmol/L L-glutamine, 100 U/mL penicillin, and 10 mg/mL streptomycin (Gibco BRL, Burlington, ON, Canada). tsA201 cells were grown in high-glucose DMEM supplemented with 10% FBS, 2 mmol/L L-glutamine, 100 U/mL penicillin, and 10 mg/mL streptomycin (Gibco BRL).

For homozygous expression, Chinese hamster ovary and tsA201 cells were transfected with 500 ng of wild-type (WT) or c.896A>G mutant *HCN4* cDNA using 1.5 µL of GeneJuice transfection reagent (Sigma, Canada). To simulate the heterozygous state, cells were co-transfected with 250 ng of WT and 250 ng of c.896A>G mutant *HCN4* using 1.5 µL of GeneJuice in 25 µL of OPTI-MEM media (Invitrogen, Carlsbad, CA).

Electrophysiological Studies

Twenty-four to 48 hours posttransfection, cells emitting green fluorescence were selected for whole-cell patch clamp recordings. Transmembrane *HCN4* currents were recorded at room temperature using an Axopatch 200A amplifier (Axon Instruments, Foster City, CA). Voltage-clamp command pulses were generated using pCLAMP 10 (Axon Instruments). Currents were sampled at 10 kHz (Digidata 1440; Axon Instruments) and low-pass filtered at 1 kHz.

The patch pipette resistance was maintained between 3.5 to 4.5 MΩ, and its internal solution was comprised of (in mM): 130 KCl, 10 NaCl, 1 $MgCl_2$, 1 EGTA, 2 MgATP, and 5 HEPES, pH adjusted to 7.2 with KOH. The extracellular bath solution contained (in mM): 110 NaCl, 30 KCl, 1.8 $CaCl_2$, 1 $MgCl_2$, 5 HEPES, 1 Glucose, pH adjusted to 7.4 using NaOH. Data were digitally stored and analyzed using pClampFit 10.3 and Prism 3.03 (GraphPad Software Inc., San Diego, CA). To obtain I-V relationships, *HCN4* currents were elicited by 4-ms voltage steps ranging from −160 to 0 mV in 20 mV increments from

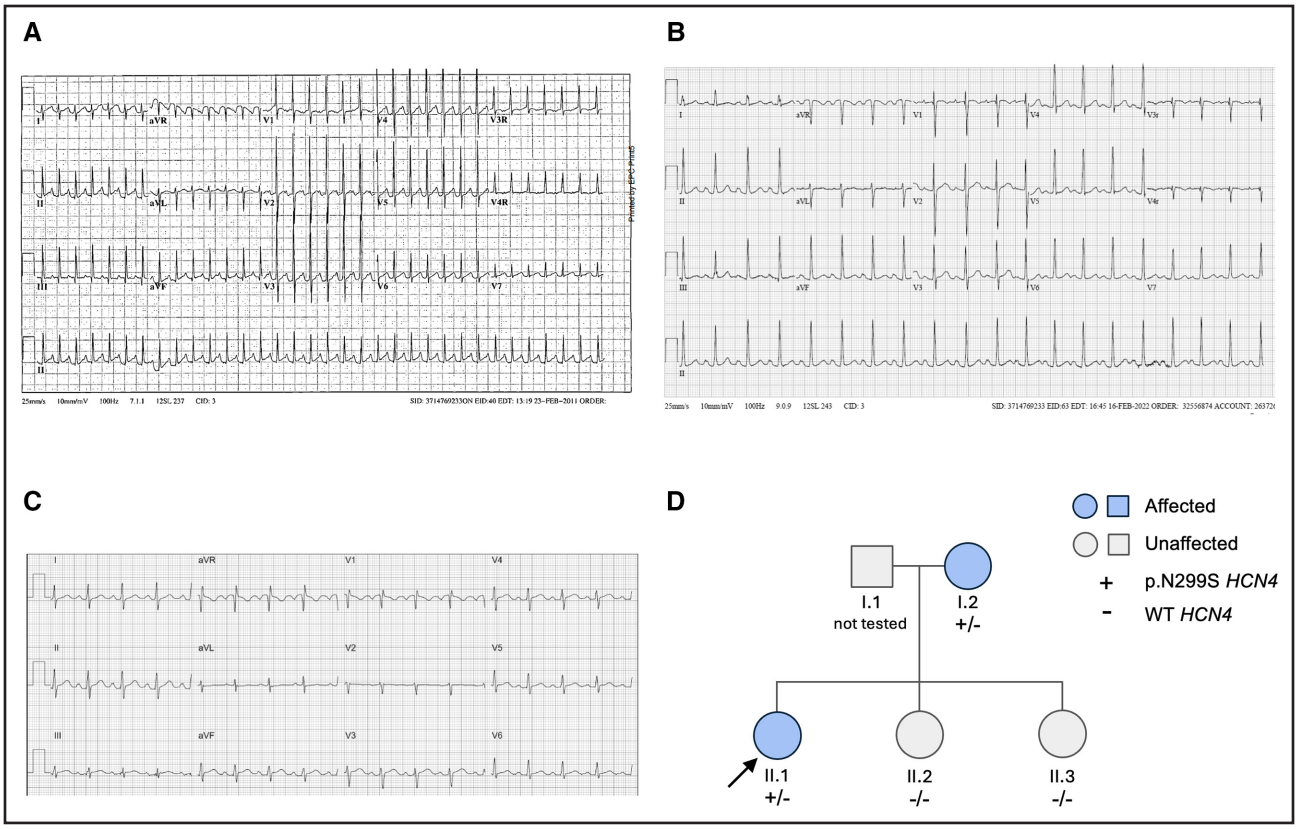

Figure 1. Representative ECGs and Pedigree.
A, Archived ECG of the index case at 2 weeks of age showing inappropriate sinus tachycardia (IST) of 200 bpm at rest. **B**, Resting ECG of index case at age 11 years off medications showing sinus tachycardia at 115 bpm. **C**, Resting ECG of the mother of the index case at age 44 years showing IST of 105 bpm. **D**, Pedigree of the family of a mother and daughter with IST. The arrow indicates the index case (daughter). WT indicates wild-type.

a holding potential of −40 mV. In a subset of experiments, current densities at −140 mV were measured in WT, p.N299S, or WT/p.N299S cells before and after application of 3 μM ivabradine.

Non−steady-state activation curves were constructed by plotting normalized tail current amplitudes elicited at 0 mV against test voltage. The fractional activation data were fitted with the Boltzmann equation: $y=1/\{1+\exp[(V-V_{50})/s]\}$, where V_{50} is the membrane potential of half-maximal activation and S is the slope of the activation curve. Non−steady-state activation curves were generated for untreated cells and following the addition of 10 or 100 μM cAMP to the pipette solution. To obtain the reversal potentials, tail currents were elicited by applying a 5-s, −120 mV voltage step from a holding potential of −40 mV, immediately followed by a 4-s step to voltages ranging from −80 to 30 mV in 10 mV increments. Tail currents were plotted against test voltage, and the reversal potential was taken as the intersection of the linear regression with the voltage axis. The time constants of hyperpolarization-activated cyclic nucleotide-gated potassium channel current (I_{HCN4}) activation (τ_{act}) and deactivation (τ_{deact}) were obtained by fitting a monoexponential function to the activation traces at voltages ranging from −160 to −100 mV and to the tail currents elicited by the protocol used to calculate reversal potentials at voltages ranging from −50 to −100 mV, respectively.

Structural Modeling and Molecular Dynamics of the Human *HCN4* p.N299S Variant

The 3D structures of human WT and p.N299S mutant *HCN4* channels (UniprotKB id: Q9Y3Q4) were generated using the Protein Data Bank cyo-EM structures 6GYN, 6GYO, 5U6O, and 5U6P as templates, corresponding to human *HCN4* and *HCN1* channels.[9,10] Due to the large size of the entire tetrameric channel, only the coordinates corresponding to the HCN domain (HCND), the voltage sensor domain, the cyclic nucleotide binding domain (CNBD), and the C-linker domain were subjected to subsequent molecular dynamics (MD) simulations, using the PDB entry 6GYN as a template, which corresponds to the non-cAMP-bound form. The structure of the PDB entry 6GYO, corresponding to the *HCN4* channel in complex with cAMP, was used for comparison. The voltage sensor structural subdomain, where the p.N299S variant is located, extends from S259 at the start of alpha helix S1 to Y409 at the end of alpha helix S4.[9]

Once modeled, the coordinates corresponding to the WT and variant domains were subjected to 200 ns of unrestricted MD simulation using the Amber18 package (https://ambermd.org; University of California-San Francisco, CA), as previously described.[11] In brief, WT and variant models were first solvated with a periodic octahedral preequilibrated solvent box using the LEaP module of Amber18, with 12 Å as the shortest distance

between any atom in the protein subdomain and the periodic box boundaries. MD simulations were conducted employing the Particle Mesh Ewald method for nonbonded interactions with a cutoff distance of 8 Å. The temperature was regulated through the Langevin thermostat, maintaining a fixed temperature of 297 K with a collision frequency of 1 ps. Hydrogen bond constraints were implemented using the SHAKE algorithm, enabling a simulation time step of 2 fs. To uphold NPT conditions (constant number of particles, pressure, and temperature), the pressure coupling was managed by a Monte Carlo Barostat set to 297 K and 1 bar. The initial model structures underwent 10 000 cycles of energy minimization, followed by a 1 ns restrained equilibration phase, smoothly raising the temperature to 297 K, after which restraints were gradually removed over 10 ns. Subsequently, each system was subjected to a 200 ns-long free MD production phase. Trajectories were analyzed using cpptraj[12] and VMD.[13] Figures were generated with Pymol (https://pymol.org).

Statistical Analysis

Data are expressed as the mean±SEM. Activation curves and current densities were statistically analyzed using the Kruskal-Wallis test followed by Dunn's Multiple Comparison test. A Mann-Whitney *U* test was used for comparison of activation V_{50} in the absence and presence of cAMP. For comparisons of activation and deactivation time constants and of reversal potentials in WT and p.N299S mutant cells, 2-tailed Student *t*-tests were used for statistical analysis. $P<0.05$ was deemed statistically significant.

RESULTS

Clinical Details and Mutation Detection

We studied a family in which IST had been diagnosed in a daughter and mother (Figure 1). The index case, now 13 years of age, was detected in utero on routine fetal ultrasound during late gestation to have a presumed ectopic atrial tachycardia with heart rates exceeding 200 bpm. Following delivery, tachycardia persisted, again considered to represent atrial tachycardia (Figure 1A). During her first 6 years of life, she was managed with oral sotalol 3 mg/kg per day with a modest reduction in heart rate, with ECGs most consistent with IST. Sotalol therapy was discontinued at age 11 years, and routine follow-up thereafter continued to document sinus rates in the range of 105 to 115 bpm (Figure 1B). Holter monitoring at age 11 years showed an average heart rate of 100 bpm (range of 62–111 bpm). Consideration of a genetic cause for her phenotype, which now included mild left ventricular dysfunction, led to broad panel genetic testing of 62 genes associated with arrhythmia and cardiomyopathy in a certified, commercial laboratory. A heterozygous variant in the *HCN4* gene was identified, p.N299S (c.896A>G), classified as a variant of unknown significance. The N299 *HCN4* amino acid residue is located within the second (S2) transmembrane helix of the protein and is highly conserved across all mammalian species and other isoforms of the HCN gene family (https://blast.ncbi.nlm.nih.gov/Blast.cgi?PAGE=Proteins). The patient was then commenced on oral ivabradine twice daily (5 mg/2.5 mg), showing significant improvement in resting heart rate (87 bpm; Figure 2A) and normalization of left ventricular function on echocardiography. Clinical and genetic assessment was performed in both sisters of the proband and showed normal ECG and Holter heart rate parameters, and absence of genetic carrier status. Clinical assessment of both parents was then undertaken, noting a resting heart rate of 110 bpm in her asymptomatic, 44-year-old mother. Holter monitoring of the mother noted an average heart rate of 100 bpm, and a minimum heart rate during sleeping hours of 77 bpm. Rapid, wide complex rhythm often competed with sinus-driven rhythm, suggesting enhanced automaticity of junctional tissue, in addition to IST (Figures 1C and 2B). Genetic testing confirmed the presence of the *HCN4* variant. Initiation of ivabradine at 5 mg twice daily resulted in improved sinus rates (85 bpm at rest and an average heart rate on Holter of 85 bpm) and resolution of junctional-driven rhythm. Subsequent addition of bisoprolol 2.5 mg daily reduced the resting heart rate of the mother to 65 bpm, with Holter showing an average heart rate of 75 bpm.

Electrophysiological Studies

WT and p.N299S-*HCN4* channels were expressed in Chinese hamster ovary or tsA201 cells and functionally assessed by whole-cell patch clamp analysis. I_{HCN4} generated by cells expressing p.N299S was significantly increased as compared with WT cells in the −160 to −120 mV range (Figure 3), and peak current density was increased by 113% (−209.15±26.71 mV versus −98.28±9.99 mV; $P<0.05$; Table 1). In cells co-expressing WT and p.N299S *HCN4* (p.N299S/WT), simulating heterozygosity, I_{HCN4} remained significantly elevated, with a 69% increase in peak current density compared with that of WT cells (−166.45±15.32 mV versus −98.28±9.99 mV; $P<0.05$; Table 1). No differences in the reversal potential of I_{HCN4} were observed (Figure 4B). Treatment of p.N299S/WT or p.N299S *HCN4*-expressing cells with the *HCN4* channel blocker ivabradine (3 μM) restored the elevated mutant I_{HCN4} densities to WT levels (Figure 3D and 3E).

p.N299S mutant channels activated faster and deactivated slower than WT channels, as indicated by the plots of mean τ_{act} and τ_{deact} obtained at different membrane potentials in Figure 3C and 4C, respectively. As compared with WT cells, τ_{act} values were significantly faster at −160, −140, and −120 mV in cells expressing mutant channels ($P<0.05$), while τ_{deact} was significantly slower at −40, −20, and 30 mV ($P<0.05$).

Voltage-dependent activation properties of WT, p.N299S/WT, and p.N299S *HCN4* channels were examined by analyzing I_{HCN4} tail currents, as previously described.[3,4] In both p.N299S/WT- and p.N299S-*HCN4*

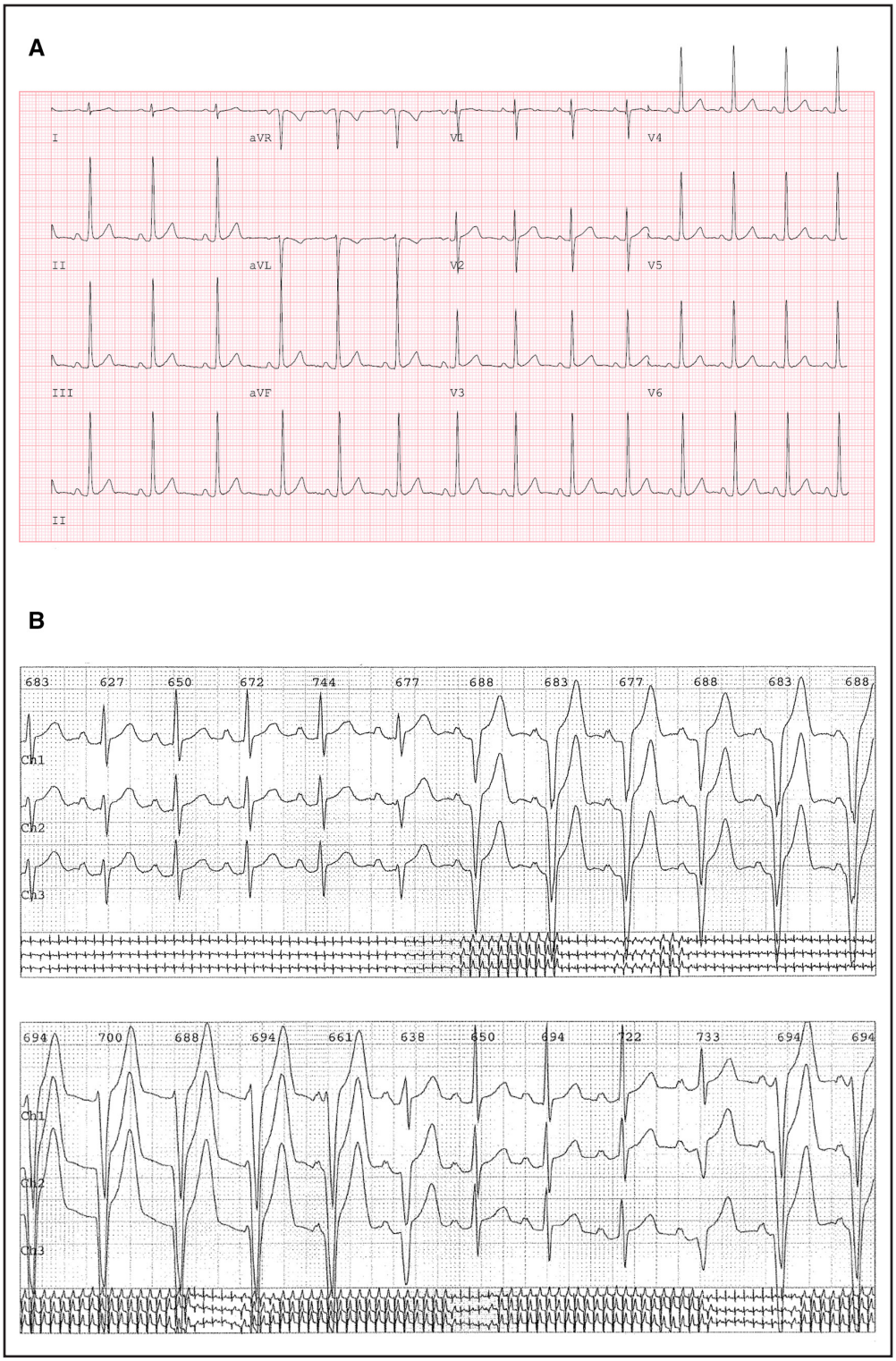

Figure 2. ECGs of affected cases.
A, Resting ECG of the index case at age 12 years while on ivabradine twice daily (5 mg/2.5 mg) with heart rate of 85 bpm. **B**, Representative tracings from a Holter monitor of the mother showing automatic low junctional rhythm competing with sinus rhythm during sleeping hours. HR indicates heart rate.

expressing cells, the voltage-dependency of *HCN4* channel activation (Figure 5B) and half-maximal activation voltages (V_{50}) were shifted towards more depolarized values as compared with cells expressing WT *HCN4* (V_{50} values of −72.21±3.96 mV in WT, −57.02±2.37 mV in p.N299S/WT, and −55.75±2.76 mV in p.N299S cells, $P<0.05$ for WT versus p.N299S/WT and for WT versus p.N299S; Table 1).

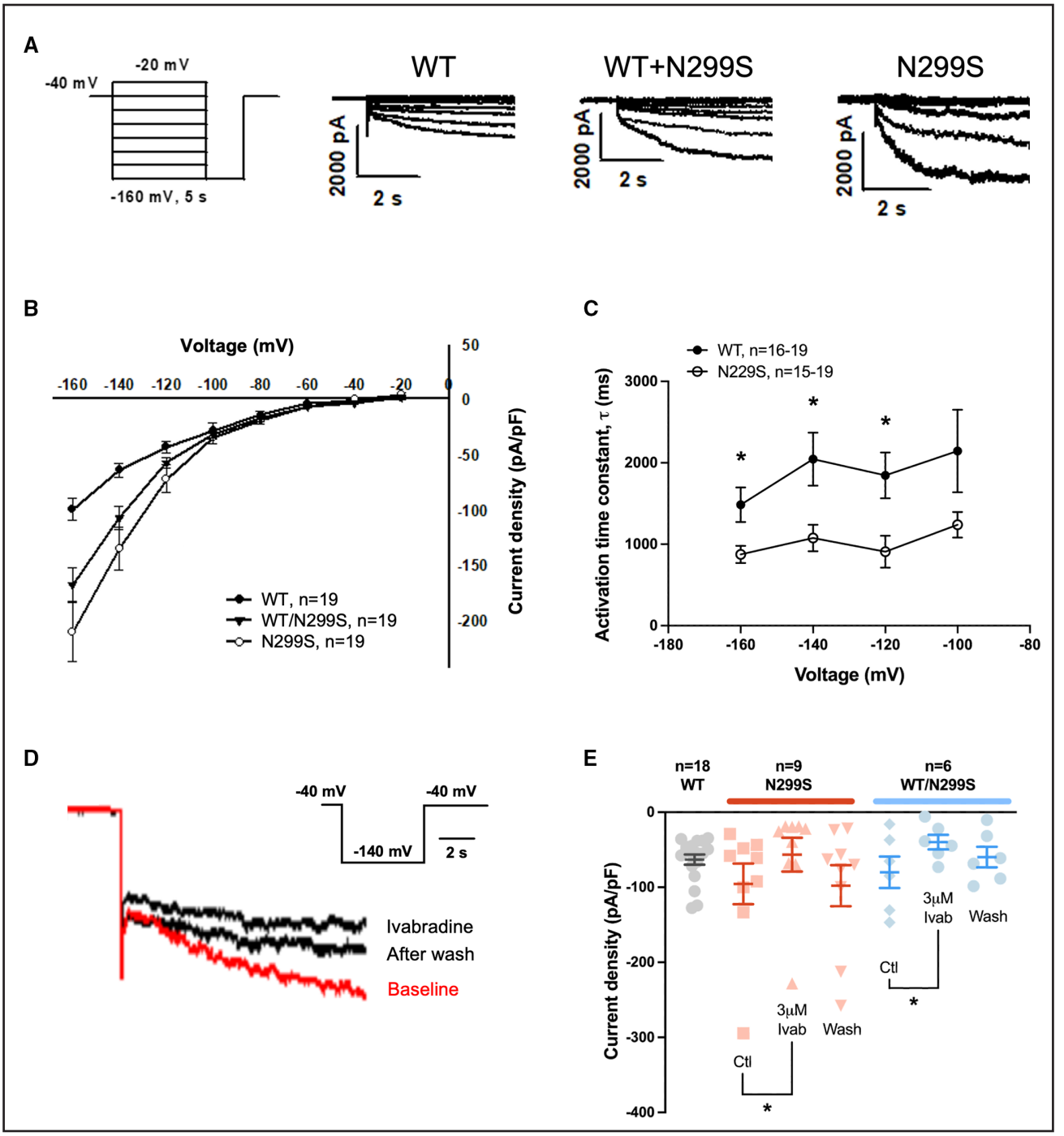

Figure 3. Electrophysiologic traces recorded in Chinese hamster ovary cells expressing wild-type (WT), WT/p.N229S, and p.N229S HCN4 cDNA.

A, Voltage protocol used to obtain current density (left) and representative traces recorded in Chinese hamster ovary cells expressing wild-type (WT), WT/p.N229S, and p.N229S *HCN4* cDNA (right). **B**, Current density-voltage relationships in WT, WT/p.N229S, and p.N229S cells. **C**, Time constants of I_{HCN4} activation (τ) of WT (filled circles) and p.N299S (open circles)-expressing cells obtained by fitting the activation phase of current density traces with a monoexponential function at voltages of −160, −140, −120, and −100 mV. **D**, Voltage protocol (**top**) and representative traces (**bottom**) before, during application, and after wash-out of 3 μmol/L ivabradine. **E**, Average I_{HCN4} densities generated by WT cells and by WT/p.N229S or p.N229S mutant cells before, during application, and after wash-out of 3 μmol/L ivabradine (Ivab). Data are represented as the mean±SEM. *P<0.05.

Interestingly, the I_{HCN4} activation curves obtained from cells expressing p.N299S/WT or p.N299S *HCN4* channels in the absence of the channel activating agent cAMP were nearly identical to the curve constructed from WT cells treated with a saturating concentration of cAMP (100 μM; Figure 5C and 5D), suggesting that the

Table 1. Voltage-Dependent Properties of Cells Expressing p.N299S Mutant and Wild-Type *HCN4 cDNA*

	WT	WT/p.N299S	p.N299S
Current density at −160 mV (pA/pF)	−98.28±9.99	166.45±15.32*	−209.15±26.71*
	n=19	*n*=19	*n*=19
Activation properties			
V_{50} (mV)	−72.21±3.96	−57.02±2.37*	−55.75±2.76*
	n=14	*n*=14	*n*=11
Slope (k_{act})	−22.94±1.74	−23.04±0.82	−19.26±0.98
	n=14	*n*=14	*n*=11
Activation properties in the presence of cAMP (100 µM)			
V_{50} (mV)	−55.6±5.18†	−50.29±2.4	−47.12±4.63
	n=6	*n*=12	*n*=5
Slope (k_{act})	−22.56±1.98	−21.83±1.14	−18.61±1.08
	n=6	*n*=12	*n*=5

All experiments were performed at room temperature. Data are represented as the mean ± SEM. For comparisons between WT, WT/p.N299S, and p.N299S cells, statistical significance was evaluated by the Kruskal-Wallis test, followed by Dunn's Multiple Comparison tests. Statistical significance of differences between activation V_{50} in the absence and presence of cAMP was evaluated by the Mann-Whitney *U* test. V_{50} indicates voltage of half-maximal activation; and WT, wild-type.

*$P<0.05$ vs WT.

†$P<0.05$ vs in the absence of cAMP.

p.N299S variant mimics the effect of cAMP-mediated activation in the absence of nucleotide. The effect of cAMP on mutant *HCN4* channels was insignificant compared with WT channels, only producing statistically significant enhancement of steady-state activation in cells expressing WT *HCN4*, suggesting a tendency to constitutive activation in mutant channels in the absence of cAMP modulation ($P<0.05$; Table 1; Figure 5G).

Structural Modeling and MD of Human *HCN4* N299S Variant

The initial structure subjected to MD simulation was obtained from the coordinates described for the human *HCN4* channel in its non-cAMP-bound state (PDB: 6GYN; Figure 6A and 6B), containing the voltage sensor domain, the HCND, and the cytosolic CNBD/C-linker domains. The structure of the domain containing the p.N299S variant was obtained by direct substitution of the N299 side chain for serine in the WT domain model. The models were simulated for 200 ns using MD techniques to analyze the effect of the variant on the structure of the voltage sensor and on the interaction between the voltage sensor, the CNBD/C-linker and the HCND, and the changes in the structure were continuously monitored. The results are shown in Figure 6.

After 200 ns of free MD simulation of the WT voltage sensor (Figure 6D), it can be observed that the domain structure remains largely unchanged, closely resembling its initial state, with very small fluctuations in the root mean square deviation values measured along the trajectory (Figure 6C, green). In this state, N299 is part of a group of residues that keep helices S1 (I280), S2 (W295, I296, N299, V300, D303) and S4 (R387) in physical contact. This arrangement does not change significantly during the 200 ns of MD.

In the case of the voltage sensor domain containing the p.N299S variant, the situation is different. During the 200 ns of MD, the structure of the voltage sensor changes more significantly than the WT domain structure, showing root mean square deviation measurements with larger oscillations, reaching values of up to 4 Å at certain times (Figure 6C, red). An analysis of the position of S299 and the surrounding amino acids shows that, throughout the dynamics, this structure exhibits positions where helix S2, in which S299 is located, separates from contact with helices S1 and S4, modifying the structure of the entire voltage sensor domain (Figure 6E).

Striking similarities were observed between the structure of the voltage sensor containing the p.N299S variant and that of the WT channel in complex with cAMP (Figure 6F). Consistent with that of p.N299S *HCN4* channels, the voltage sensor of the cAMP-bound protein also shows separation of the S2 helix from helices S1 and S4.

Modulation of voltage gating by cAMP relies on mechanical coupling between the voltage sensor, the HCND, and the CNBD/C-linker domains.[9,14,15] In the WT *HCN4* channel model corresponding to the ligand-free state (PDB: 6GYN), the interface between the HCND and the CNBD remained stable after 200 ns of simulation, and the shortest distance between alpha carbons of each domain (residues S23 of the HCND and G396 of the CNBD, taken only as a distance reference) remained around 5.5 Å (Figure 6G). In contrast, in the p.N299S mutant channel (Figure 6H), and due to conformational change at the interface between the 3 domains, the distance between alpha carbons S23 and G396 increased markedly, to 7.2 Å by the end of the simulation. In the case of the WT channel model in the presence of cAMP (PDB: 6GYO), this distance increases to 6.8 Å (Figure 6I), aligning with the trend observed in the mutant structure. These results are consistent with the electrophysiological characteristics of mutant channels and suggest that, in the absence of cAMP, the p.N299S variant shifts the equilibrium conformation of the *HCN4* protein to a position analogous to that of WT channels reached after binding to the nucleotide.

DISCUSSION

In this study, we describe a mutation in the *HCN4* gene associated with familial IST, electrophysiologically characterized to cause constitutive activation of the channel. The index case was diagnosed pre- and postnatally with ectopic atrial tachycardia, ultimately recognized to represent IST. Her mother was similarly recognized to have

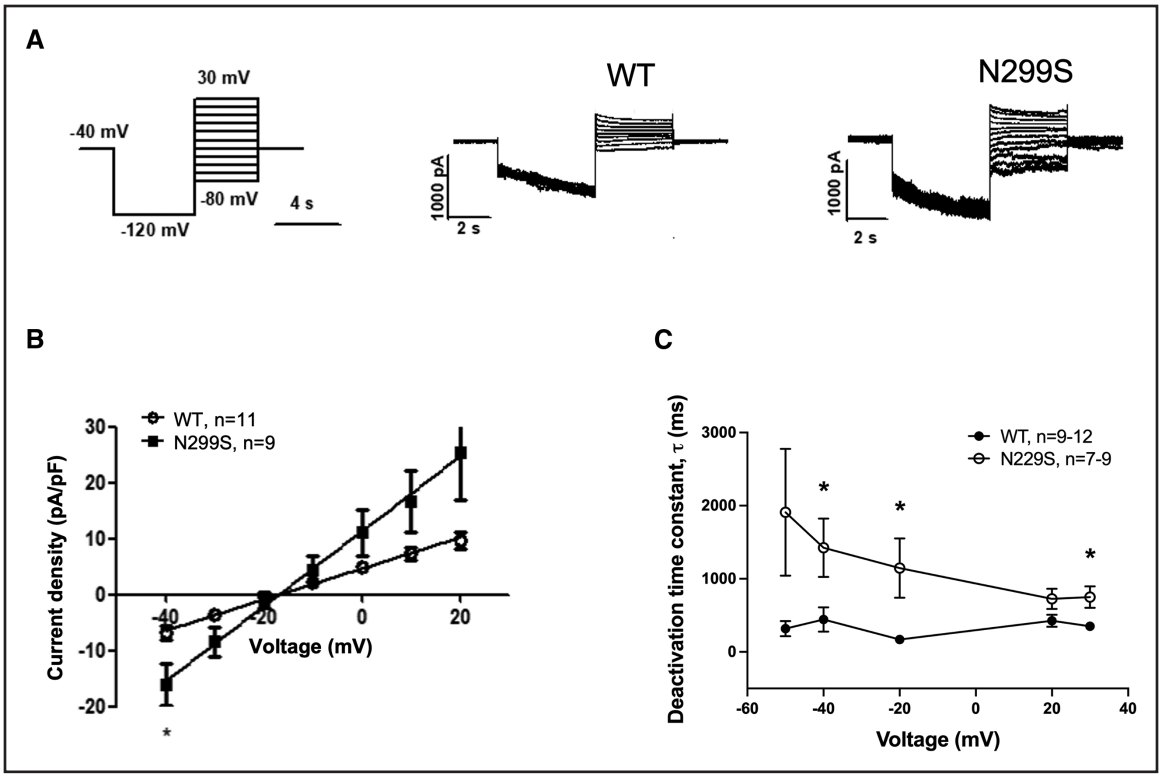

Figure 4. p.N299S-*HCN4* significantly slows channel deactivation without affecting the reversal potential.
A, Voltage protocol for obtaining reversal potentials and time constants of I_{HCN4} deactivation (τ). A 5-s, −120 mV prepulse was delivered from a holding potential of −40 mV, followed by a series of 4-s test pulses ranging from −80 mV to +30 mV at 10 mV increments to elicit tail currents, then the voltage was stepped back to the holding potential (**left**). Representative traces recorded from *HCN4* WT and p.N299S cells are shown on the **right**. **B**, Tail current density-voltage relationships. Intersection of the linear regression fits with the voltage axis indicates the reversal potential (−20 mV for both wild type [WT] and mutant channels). **C**, Deactivation time constants obtained by monoexponential fitting of the tail currents. Data are presented as the mean±SEM. **P*<0.05.

IST and was identified as a mutation carrier. This variant, p.N299S, mimics the structural and electrophysiological effects of cAMP binding to *HCN4*, effectively replicating the mechanism through which cAMP enhances channel activity.

The index case showed minimal response to sotalol therapy and eventually developed mild impairment of left ventricular function by age 11 years. Treatment with ivabradine led to improved control of IST and resolution of left ventricular dysfunction. Similarly, the mother of the child, although predominantly asymptomatic aside from general fatigue, demonstrated normalized heart rate behavior and resolution of junctional arrhythmias with ivabradine and low-dose bisoprolol.

The identified p.N299S variant causes a robust gain of *HCN4* channel function, producing a large increase in I_{HCN4} density that could be returned to WT-levels by ivabradine. Expression of both heterozygous and homozygous mutant p.N299S-*HCN4* significantly depolarized the voltage-dependency of *HCN4* activation, and I_{HCN4} generated by mutant channels activated faster and deactivated slower than that generated by WT channels. These effects are consistent with the mechanisms by which cAMP augments *HCN4* activity,[6,7] suggesting that the p.N299S mutation either increases sensitivity to cAMP or alters intrinsic channel properties, mimicking the effects of cAMP in the absence of nucleotide.

The first genetic variant to be associated with IST, a p.R524Q substitution in the *HCN4* C-linker domain, was described by Baruscotti et al in 2017.[3] Unlike the variant reported in our family, the p.R524Q variant had no difference in baseline I_{HCN4} density compared with WT channels. However, the authors elucidated a significantly increased affinity and sensitivity for cAMP as being responsible for the positive activation curve shift observed in mutant channels,[3] consistent with the location of R524 within the C-terminal region known to couple cAMP binding to channel activation.[16] The only other reported *HCN4* variant to be associated with IST is p.V240M,[4] located within the N-terminal HCND region of the channel. This domain is recognized to contribute to stabilizing the closed state of the pore for HCN channels.[9] Not surprisingly, these investigators demonstrate that p.V240M induces a gain-of-function in I_{HCN4} through enhancing the open probability of the channel, and not through increased cAMP sensitivity, which remained similar to WT channels.[4] Uniquely, we

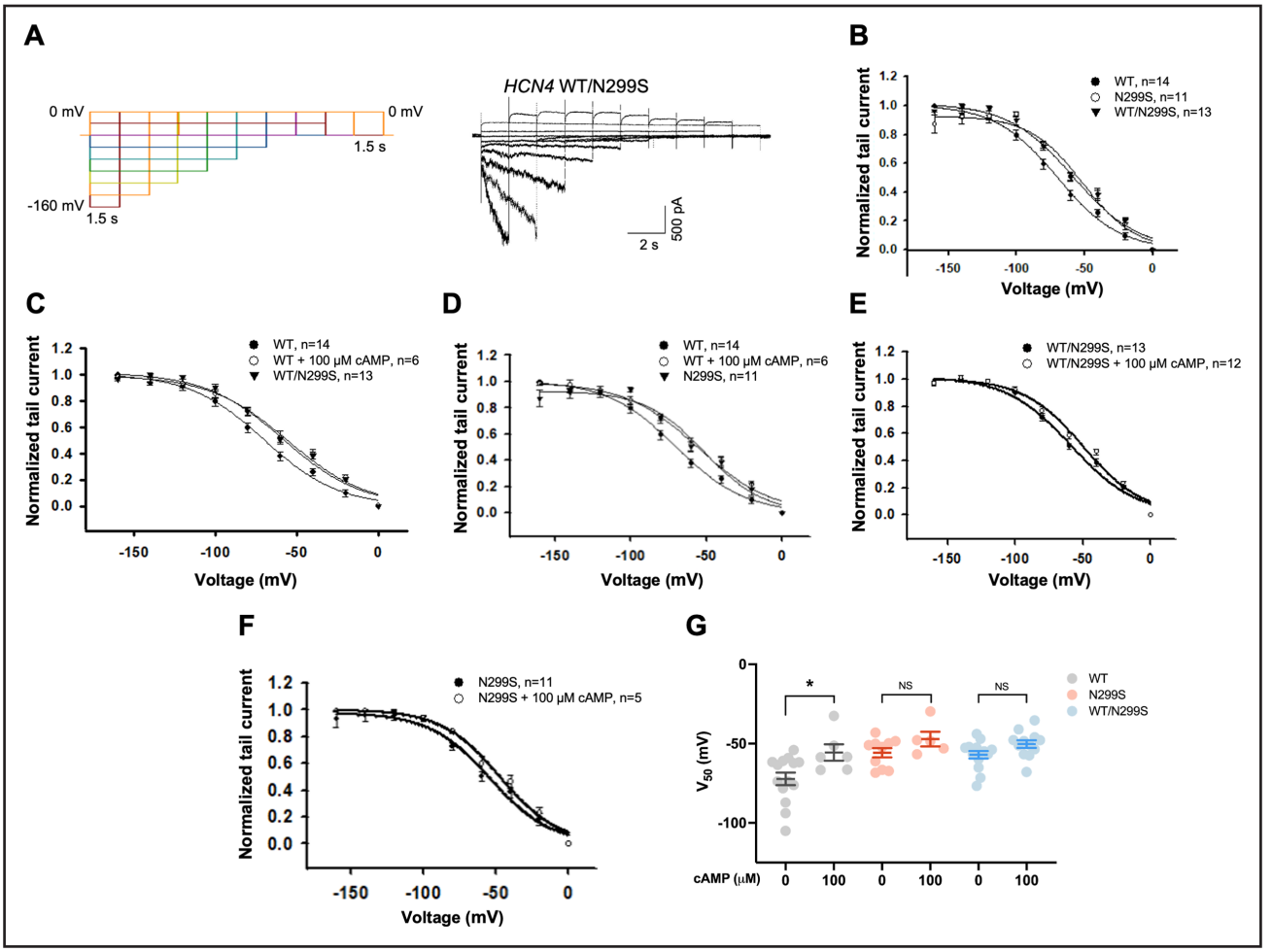

Figure 5. Effects of the p.N299S mutation on voltage-dependent activation and responsiveness to cAMP in TSA201 cells. **A, Left**: Voltage protocol used to study voltage-dependent activation. A series of 1.5-s test pulses was delivered from a holding potential of −40 mV, then the voltage was stepped to 0 mV for 1.5 s to elicit tail currents and then stepped back to the holding potential. The test pulses started at −160 mV, applied at 20 mV increments. **Right**: Representative trace elicited by wild-type (WT)/N299S channels using the voltage protocol on the **left**. **B**, Voltage dependence of activation curves of WT, WT/p.N229S, and p.N229S cells constructed by Boltzmann fits of the normalized tail currents against the membrane potentials of the test pulse. The WT/p.N299S and p.N299S activation curves were significantly shifted to the right as compared with WT cells. **C**, Voltage dependence of activation curves of WT cells in the presence and absence of 100 µmol/L cAMP and superimposed activation curves of WT/p.N229S, and (**D**) p.N229S mutant cells. Note that expression of mutant *HCN4* channels induces rightward activation curve shifts that are nearly identical to those caused by the application of cAMP to WT cells. **E**, Voltage dependence of activation curves of WT/p.N229S cells at baseline and in the presence of 100 µmol/L cAMP. **F**, Voltage dependence of activation curves of p.N299S cells at baseline and in the presence of 100 µmol/L cAMP. **G**, Half-maximal activation voltages (V_{50}) at baseline and in the presence of 100 µmol/L cAMP in cells expressing WT, WT/p.N229S, and p.N229S *HCN4*. Application of cAMP elicits statistically significant depolarization of the V_{50} in WT, but not WT/p.N229S or p.N229S mutant cells. Sample sizes for (**G**) as noted in Table 1. Data are presented as the mean±SEM. *P<0.05.

demonstrate I_{HCN4} gain-of-function through yet another unique mechanism, as 3D structural modeling demonstrates that p.N299S-*HCN4* channels are intrinsically in a state of sub-maximal cAMP activation, with minimal responsiveness to cAMP as compared with WT channels (see Table 2).

The p.N299S variant affects a residue in the transmembrane S2 helix of the *HCN4* voltage sensor domain. Reconstructions of the WT voltage sensor generated by MD simulations showed that residue N299 is part of a stable cluster of residues that keep helices S1, S2, and S4 in physical contact (I280 of S1, W295, I296, N299, V300, D303 of S2, and R387 of S4). In the case of the mutant, the voltage sensor underwent a substantial conformational change, and analysis of the positions of S299 and the surrounding amino acids showed that, throughout dynamics, the structure exhibits positions where helix S2 separates from contact with helices S1 and S4, dramatically modifying the structure of the entire voltage sensor. Importantly, cAMP-induced modulation of HCN channel gating involves upwards displacement of the voltage sensor and structural

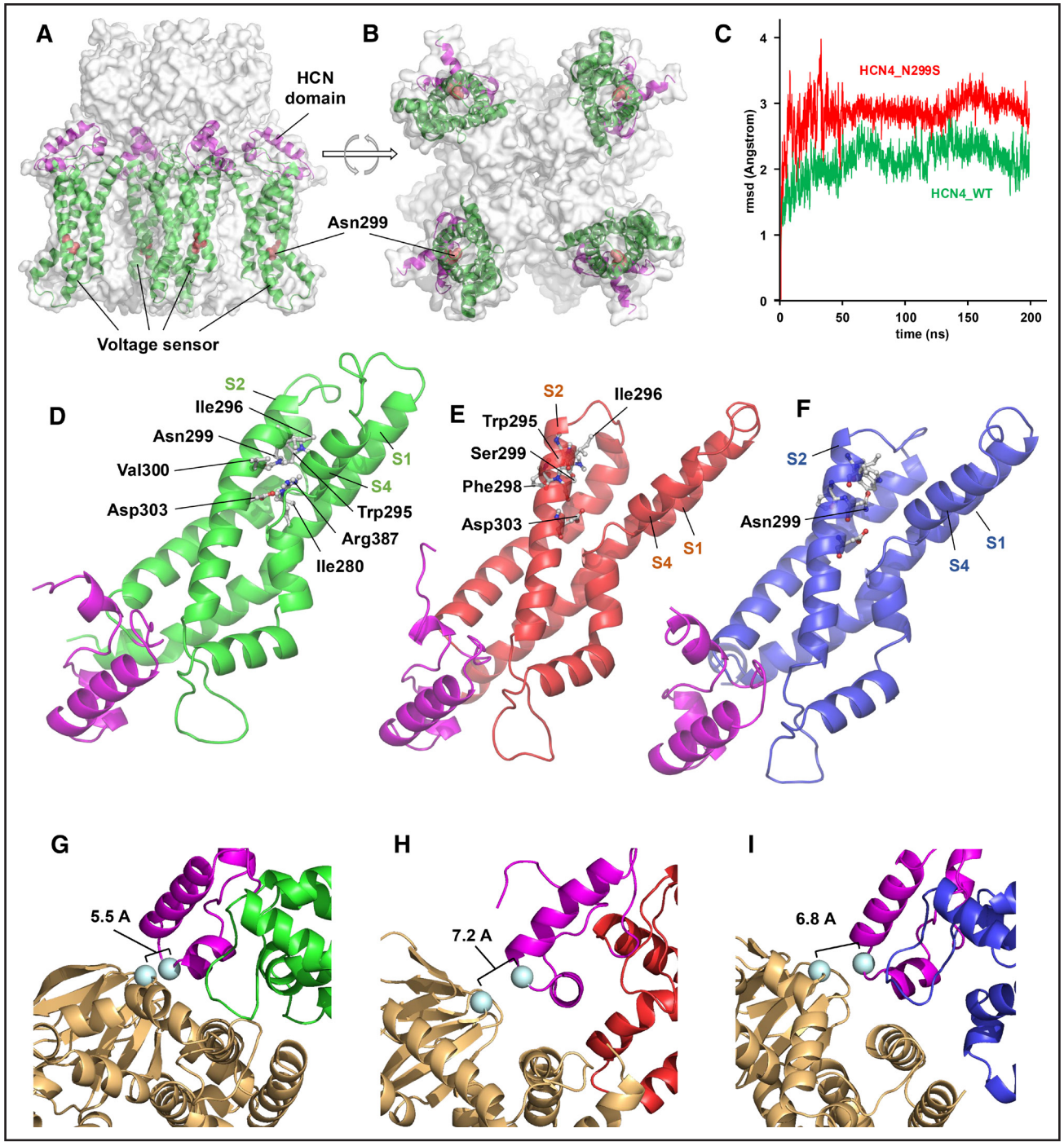

Figure 6. Effect of the p.N299S variant on the 3D structure model of human *HCN4*.
A, Lateral and (**B**) bottom view of the structure of the human *HCN4* channel tetramer. The voltage sensor domains are represented in green, and the HCN domains (HCNDs) in magenta. The position of amino acid Asn299 (red spheres) on the inner voltage sensor domain surfaces is indicated. **C**, Root mean square deviation plots (in Å) measured along 200 ns molecular dynamics trajectories of the wild-type (WT, green) and p.Asn299Ser mutant (red) voltage sensor domains. **D**, Structure of the voltage sensor domain of the WT *HCN4* protein after molecular dynamics simulation. The position of the helices S1, S2, and S4, as well as the amino acids that form a stable cluster around Asn299, are shown (Ile280, Trp295, Ile296, Asn299, Val300, Asp303, Arg387). **E**, Structure of the p.Asn299Ser mutant voltage sensor following molecular dynamics simulation. The position of helices S1, S2, and S4 is indicated. The position of residues in the S2 helix that remain close to Ser299, but separate from S4, are also shown (Trp295, Phe298, Ser299, Asp303). **F**, Structure of the WT voltage sensor domain in the cAMP-bound state. The positions of helices S1, S2, and S4 and the Asn299 residue are indicated. **G**, Structure of the interface between the cyclic nucleotide binding domain (CNBD)/C-linker domains (ochre) and the HCND (magenta) of WT *HCN4* after 200 ns of molecular dynamics simulation. The distance between the alpha carbons of amino acids Ser23 of the HCND and Gly396 of the CNBD (cyan spheres) is indicated. **H**, Interface between the CNBD/C-linker (ochre) and the HCND of p.Asn299Ser-*HCN4* (red) after molecular dynamics simulation. The distance between the alpha carbons of Ser23 and Gly396 is indicated. **I**, Structure of the same interface as in (**G**) and (**H**), corresponding to the WT *HCN4* channel crystallized in the presence of cAMP. The distance between Ser23 and Gly396 is shown.

Table 2. Localization and Electrophysiological Properties of the p.N299S, p.V240M, and p.R524Q *HCN4* Variants

	p.R524Q	p.V240M	p.N299S
Domain affected	C-linker domain (modulator of cAMP binding)	HCND (stabilizes the closed state)	Voltage sensor domain (TM2)
Baseline *HCN4* current density	No change	Increased	Increased
cAMP sensitivity	Increased response compared with WT channels	Similar cAMP response as WT channels	Reduced responsiveness to cAMP compared with WT channels
Mechanism of GOF	Increased channel sensitivity to cAMP	Demonstrated increased channel open probability	Structural mimicry of the cAMP-bound state

Comparison of the protein domain location and the demonstrated biophysical and structural effects of the *HCN4* variants p.N299S, p.R524Q, and p.V240M. GOF indicates gain-of-function; HCND, HCN domain; and TM2, second transmembrane domain.

rearrangements of the voltage sensor helices that favor channel opening.[9,10,15] Functional evidence and the relatively recently published high-resolution structures of *HCN1* and *HCN4* have demonstrated that these conformational changes are transmitted to the voltage sensor by movements of the cytosolic CNBD/C-linker and the HCND, and that these domains physically interact.[9,10,14,15] If p.N299S-*HCN4* channels intrinsically mimic the effect of cAMP, the equilibrium conformation of the mutant voltage sensor would be expected to resemble that of the WT channel in complex with the nucleotide and be associated with conformational change of the CNBD-voltage sensor interface with the HCND. Indeed, MD simulations revealed that the WT voltage sensor in the cAMP-bound state was strikingly similar to that of the mutant channel in the absence of cAMP, both of which demonstrated separation of the S2 helix from S1 and S4. Moreover, increased distances between alpha carbons of the HCND and CNBD (S23 and G396, respectively) in p.N299S and cAMP-bound WT *HCN4* channels relative to WT channels in the absence of cAMP indicate consistent conformational changes in the voltage sensor-CNBD-HCND interface. These data suggest that the p.N299S variant shifts the equilibrium conformation of *HCN4* channels to a state resembling that induced by cAMP and provides a structural basis for the baseline shift in the voltage dependence of activation observed in mutant cells.

CONCLUSIONS

IST is a rare condition, and only 2 mutations have previously been implicated in its pathogenesis. Here, we establish p.N299S-*HCN4* as the third variant associated with IST. Uniquely, this variant alters structural and electrophysiological properties of *HCN4* channels, mimicking the structural effect of cAMP binding and activation in the absence of the nucleotide. This study emphasizes the importance of recognizing genetic causes of IST in clinical practice, particularly in the newborn, and provides data supporting the efficacious effect of ivabradine in *HCN4* genetically based forms of this condition.

ARTICLE INFORMATION

Received March 06, 2025; accepted September 11, 2025.

Affiliations

Inherited Arrhythmia and Cardiomyopathy Program, Division of Cardiology, Department of Medicine, Toronto General Hospital, Canada (S.L.B., Q.L., T.F., M.H.G.). Department of Physiology, University of Toronto, Canada (S.L.B., Q.L., T.F., M.H.G.). Molecular Modeling Group, Centro de Biologia Molecular Severo Ochoa (CBM, CSIC-UAM), Madrid, Spain (D.R.-P., I.M.-A., P.G.-P.).

Acknowledgments

The authors are thankful to the patients for their contribution to this work. The computational support of the Centro de Computación Científica CCC-UAM is gratefully recognized.

Sources of Funding

This work was supported by a grant from the Canadian Institutes for Health Research (408226) to Dr Gollob, and a Spanish Government grant PID2021-126625OB-I00 (MCIN/AEI/10.13039/501100011033/FEDER,EU.2022) to Dr Gómez-Puertas. Dr Gollob is further supported by the Ian Copland Arrhythmia and Sudden Death Research Fund, University of Toronto.

Disclosures

None.

REFERENCES

1. Ahmed A, Pothineni NVK, Charate R, Garg J, Elbey M, de Asmundis C, LaMeir M, Romeya A, Shivamurthy P, Olshansky B, et al. Inappropriate sinus tachycardia: etiology, pathophysiology, and management: JACC review topic of the week. *J Am Coll Cardiol.* 2022;79:2450–2462. doi: 10.1016/j.jacc.2022.04.019
2. Adler A, Sadek MM, Chan AYM, Dell E, Rutberg J, Davis D, Green MS, Spears DA, Gollob MH. Patient outcomes from a specialized inherited arrhythmia clinic. *Circ Arrhythm Electrophysiol.* 2016;9:e003440. doi: 10.1161/CIRCEP.115.003440
3. Baruscotti M, Bucchi A, Milanesi R, Paina M, Barbuti A, Gnecchi-Ruscone T, Bianco E, Vitali-Serdoz L, Cappato R, DiFrancesco D. A gain-of-function mutation in the cardiac pacemaker HCN4 channel increasing cAMP sensitivity is associated with familial inappropriate sinus tachycardia. *Eur Heart J.* 2017;38:280–288. doi: 10.1093/eurheartj/ehv582
4. Cámara-Checa A, Perin F, Rubio-Alarcón M, Dago M, Crespo-García T, Rapún J, Marín M, Cebrián J, Gómez R, Bermúdez-Jiménez F, et al. A gain-of-function HCN4 mutant in the HCN domain is responsible for inappropriate sinus tachycardia in a Spanish family. *Proc Natl Acad Sci U S A.* 2023;120:e2305135120. doi: 10.1073/pnas.2305135120
5. Biel M, Wahl-Schott C, Michalakis S, Zong X. Hyperpolarization-activated cation channels: from genes to function. *Physiol Rev.* 2009;89:847–885. doi: 10.1152/physrev.00029.2008
6. Wainger BJ, Degennaro M, Santoro B, Siegelbaum SA, Tibbs GR. Molecular mechanism of cAMP modulation of HCN pacemaker channels. *Nature.* 2001;411:805–810. doi: 10.1038/35081088
7. Wicks NL, Wong T, Sun J, Madden Z, Young EC. Cytoplasmic cAMP-sensing domain of Hyperpolarization-Activated Cation (HCN) channels

uses two structurally distinct mechanisms to regulate voltage gating. *Proc Natl Acad Sci U S A*. 2011;108:609–614. doi: 10.1073/pnas.1012750108
8. Edelheit O, Hanukoglu A, Hanukoglu I. Simple and efficient site-directed mutagenesis using two single-primer reactions in parallel to generate mutants for protein structure-function studies. *BMC Biotechnol*. 2009;9:61. doi: 10.1186/1472-6750-9-61
9. Lee CH, MacKinnon R. Structures of the human HCN1 hyperpolarization-activated channel. *Cell*. 2017;168:111–120.e11. doi: 10.1016/j.cell.2016.12.023
10. Saponaro A, Bauer D, Giese MH, Swuec P, Porro A, Gasparri F, Sharifzadeh AS, Chaves-Sanjuan A, Alberio L, Parisi G, et al. Gating movements and ion permeation in HCN4 pacemaker channels. *Mol Cell*. 2021;81:2929–2943.e6. doi: 10.1016/j.molcel.2021.05.033
11. Ros-Pardo D, Gómez-Puertas P, Marcos-Alcalde I. STAG2: computational analysis of missense variants involved in disease. *Int J Mol Sci*. 2024;25:1280. doi: 10.3390/ijms25021280
12. Roe DR, Cheatham TE. PTRAJ and CPPTRAJ: software for processing and analysis of molecular dynamics trajectory data. *J Chem Theory Comput*. 2013;9:3084–3095. doi: 10.1021/ct400341p
13. Humphrey W, Dalke A, Schulten K. VMD: visual molecular dynamics. *J Mol Graph*. 1996;14:33–38. doi: 10.1016/0263-7855(96)00018-5
14. Porro A, Saponaro A, Gasparri F, Bauer D, Gross C, Pisoni M, Abbandonato G, Hamacher K, Santoro B, Thiel G, et al. The HCN domain couples voltage gating and cAMP response in hyperpolarization-activated cyclic nucleotide-gated channels. *Elife*. 2019;8:e49672. doi: 10.7554/eLife.49672
15. Saponaro A, Thiel G, Moroni A. Structural and functional approaches to studying cAMP regulation of HCN channels. *Biochem Soc Trans*. 2021;49:2573–2579. doi: 10.1042/BST20210290
16. Zagotta WN, Olivier NB, Black KD, Young EC, Olson R, Gouaux E. Structural basis for modulation and agonist specificity of HCN pacemaker channels. *Nature*. 2003;425:200–205. doi: 10.1038/nature01922